HHS Public Access

Author manuscript

Int J Radiat Oncol Biol Phys. Author manuscript; available in PMC 2017 November 01.

Published in final edited form as:

Int J Radiat Oncol Biol Phys. 2016 November 1; 96(3): 696–705. doi:10.1016/j.ijrobp.2016.07.010.

Effect of the Maximum Dose on White Matter Fiber Bundles Utilizing Longitudinal Diffusion Tensor Imaging

Tong Zhu, Ph.D.[1], **Christopher H. Chapman, MD.**[1], **Christina Tsien, MD.**[2], **Michelle Kim, MD.**[1], **Daniel E. Spratt, MD**[1], **Theodore S. Lawrence, MD., Ph.D.**, and **Yue Cao, Ph.D.**[1,3,4]

[1]Department of Radiation Oncology, University of Michigan, Ann Arbor, Michigan, USA

[2]Department of Radiation Oncology, Washington University at St. Louis, St Louis, Missouri, USA

[3]Department of Radiology, University of Michigan, Ann Arbor, Michigan, USA

[4]Department of Biomedical Engineering, University of Michigan, Ann Arbor, Michigan, USA

Abstract

Purpose—Previous efforts to decrease neurocognitive effects of radiation focused on sparing isolated cortical structures. We hypothesize that understanding temporal, spatial and dosimetric patterns of radiation damage of whole brain white matter (WBWM) after partial brain irradiation might also be important. Therefore, we carried out a study to develop the methodology to assess radiotherapy-induced damage to WBWM bundles.

Methods—An atlas-based, automated WM tractography analysis was implemented to quantify longitudinal changes in indices of diffusion tensor imaging (DTI) of 22 major WM fibers in 33 patients with predominantly low-grade/benign brain tumors treated by radiotherapy. Six DTI scans per patient were performed from pre-RT to 18 months post-RT. The DTI indices and planned doses (maximum and mean doses) were mapped onto profiles of each of 22 WM bundles. A multivariate linear regression was performed to determine the main dose effect as well as the influence of other clinical factors on longitudinal percentage changes in axial and radial diffusivity (AD and RD) from pre-RT.

Results—Of 22 fiber bundles, AD/RD changes in 12 bundles were affected significantly by doses ($P<0.05$), as the effect was progressive over time. In nine elongated tracts, decreased AD/RD was significantly related to maximum doses received, consistent with a serial-structure. In individual bundles, AD changes were up to 11.5% at the maximum dose locations 18 months post-RT. The dose effect on WM was greater in older females than younger males.

Conclusion—Our study demonstrates for the first time that the maximum dose to the elongated WM bundles causes post-radiotherapy damage in WM. Validation and correlative studies are

Corresponding author: Yue Cao, Ph.D., Department of Radiation Oncology, University of Michigan, 519 W Williams St, Ann Arbor, MI 48103, Tel: 734-647-2914, yuecao@umich.edu.

necessary to determine the ability and impact of sparing these bundles on preserving neurocognitive function post-radiotherapy.

Keywords

radiation-induced white matter damage; diffusion tensor imaging; reactive astrogliosis; axonal injury; dose-response pattern; atlas-based fiber tractography

Introduction

Radiation therapy (RT) is part of standard care for patients with numerous types of benign and malignant brain tumors. However, RT, including partial brain RT, has been shown to cause neurocognitive dysfunction (1-6). This often becomes apparent 6 months to years after RT, and affects a substantial percentage of patients (1-4). Longitudinal studies have revealed the progressive decline in a wide spectrum of cognitive functions in patients with low-grade glioma post RT (5, 6), which affects quality of life of long-term survivors.

Cognitive function is carried out by neural networks, supported by white matter (WM) pathways, rather than single cortical structures (i.e. the hippocampus). The network can be interrupted by damage of either functional cortices or WM fibers, resulting in cognitive dysfunction. Radiobiologic studies (2-4) have shown that radiation-induced death of neurons is minimal following clinically relevant dose. One method to clinically monitor radiation-induced changes in WM is by using diffusion tensor imaging (DTI) (7-14). DTI detects alterations in water diffusivities along and perpendicular to the long axis of axons (called axial and radial diffusivities, AD and RD). These parameters are validated as biomarkers for axonal degeneration (15-18) and demyelination (16, 18), respectively. DTI studies have been conducted in both adult and pediatric patients treated by either whole (7, 8) or partial brain RT (9-14), but only in selected WM structures, for example, corpus callosum (9) and corticospinal tracts (14). Overall, it is found that DTI changes are progressive over time and dose-dependent (9-12). Furthermore, a recent study showed a correlation between early diffusivity changes in the parahippocampal cingulum and a late decline in verbal recall (11). This suggests the potential of DTI for predicting late cognitive decline.

The regulation of neurocognitive function is complex and not fully understood. Given that neurocognitive decline is seen in multiple contexts after partial RT of various brain tumors, it raises the question of whether damage to anywhere within the network involved in cognition can induce similar dysfunction. It is plausible that subject-specific radiation damage to different sections of the same WM network could result in a similar neurocognitive outcome (Figure 1), and WM bundles could respond to a maximum radiation dose, much like a serial structure. Despite the serial-like structure of WM, most previous studies are based upon region-of-interest (ROI) analysis, which limits investigations to a portion, sometimes a small portion, of the selected bundle and results in using the mean dose within the selected volume to analyze dose response. Testing our hypothesis requires quantifying longitudinal WM changes within the entire WM network and relating them to radiation dose and specific neurocognitive outcomes.

The goal of this study was to carry out the first part of this task using an automated, robust and scalable method to extract a large quantity of WM fibers and to analyze dose-response patterns along fibers longitudinally. Specifically, we implemented an atlas-based approach, based upon deterministic DTI tractography (19), and segmented 22 major WM bundles of the whole brain of 33 patients from six time-point DTI data acquired from pre-RT to 18 months post-RT.

Methods and Materials

Study Design

Patients who underwent standard partial brain RT for low-grade or benign cranial tumors were enrolled in an IRB approved study. Inclusion criteria consisted of full completion of the study, minimal to no missing data, no major imaging artifact, and no tumor progression or severe complication (e.g., seizure, hydrocephalus or hemorrhage). This yielded 33 analyzable patients in total from study cohort.

MRI scans were performed at six time points: 1-2 weeks pre-RT, 3 and 6 weeks during RT, and 1, 6 and 18 months after RT. Nine, fifteen and nine patients had all their scans on GE 1.5T, Philips 3T and Siemens 3T scanners, respectively. All T1-weighted images had a resolution of $1\times1\times1mm^3$. DTI were acquired with (GE/Philips/Siemens): TR=9300/7073/4600ms with minimized TE, resolution=$1.25\times1.25\times4mm^3$/$1.75\times1.75\times2mm^3$/$1.72\times1.72\times3.9mm^3$, b=1000/800/1000s/$mm^2$, and the number of unique diffusion-weighting directions=9/15/20, respectively.

Atlas-based Automated White Matter Tractography Analysis

Pre-processing—DTI were corrected for bulk movements and eddy current, reformatted into a $2\times2\times2mm^3$ resolution, and calculated for fraction anisotropy (FA), AD, and RD maps using the FSL software (FMIRB Analysis Group, Oxford, UK).

Atlas-based WM Tractography—An atlas-based automated tractography analysis was developed based upon the Johns Hopkins University White Matter Tractography Atlas (JHU Atlas) (20).

The analysis included four steps (Figure 2). In the *first step*, pairwise registrations of longitudinal FA maps were performed within each patient, using an affine registration in FSL. An FA template was created from the mean image of all registered FAs. After each registration, the preservation of the principal direction algorithm (21) was applied to compensate registration-induced disturbances to tensor orientations.

In the *second step*, the FA template of each patient was registered to the standard anatomic space defined by the MNI152-T1 template, through registration of the FA template to the individual T1 images by an affine registration and followed by registration of the individual T1 images to the MNI152-T1 template by a nonlinear registration. The JHU Atlas is defined in the MNI152-T1 space, and includes 20 major WM bundles (20) and two anatomical landmark ROIs for each bundle (22). In this study, each of bilateral inferior fronto-occipital fasciculus bundles was divided into the anterior and posterior portions to maximize

repeatability of fiber tracking, resulting in 22 WM bundles. The JHU Atlas was converted into each individual's DTI space by applying the inverse transformation. The dose map, after correction to 2Gy equivalent dose per fraction (EQD2) using a linear-quadratic equation with α/β=2.5Gy, was co-registered to T1 images, through registration with the planning CT.

In the *third step*, a whole-brain tractography was first generated for each DTI using a deterministic tracking algorithm (23) with a FA threshold of 0.2. Then, each bundle was segmented by selecting fibers that went through the two ROIs from the atlas. The resultant bundle was further refined by the JHU Atlas to discard aberrant fibers. The Jaccard Similarity Index was calculated for within-patient pairs of binarized bundles at any two time points to quantify the robustness of tractography.

During the *final step*, a fiber profile was created at its center-of-mass line of the bundle. DTI and dose values along the profile were calculated with a weighted mean of corresponding values of neighboring voxels based on the Mahalanobis distance (24).

All processes were implemented in a combination of Matlab, FSL, and mrVista (Stanford University, Palo Alto, CA, USA).

Statistical Analysis

Four dosimetric metrics were calculated: averaged dose values greater than 95th, 90th and 80th percentiles of the dose-volume-histogram (DVH) along fiber profile as well as the mean dose of the bundle, referred as *95%ile, 90%ile, 80%ile* and *mean dose*. Percentage changes in AD and RD, $\Delta AD\%$ and $\Delta RD\%$, at each follow-up with respect to the pre-RT values were computed at each voxel along the fiber profile. Then, averaged values of $\Delta AD\%$ and $\Delta RD\%$ over voxels receiving doses greater than the *95%ile, 90%ile, or 80%ile*, and over all voxels along the bundle were calculated.

Longitudinal AD/RD changes in relating to dose were analyzed for each bundle at each follow-up by a linear fixed-effect model as:

$$\Delta\mathrm{AD}\%/\Delta\mathrm{RD}\% = \alpha_0 + \alpha_1 \times \mathrm{Dose} + \alpha_2 \times \mathrm{Glioma} + \alpha_3 \times \mathrm{Dose} \times \mathrm{Age} + \alpha_4 \times \mathrm{Dose} \times \mathrm{Sex} + \alpha_5 \times \mathrm{Dose} \times \mathrm{Edema} \quad (1)$$

where *Dose* is one of the four dosimetric metrics of a WM bundle as the main predictive variable. Considering that patients with glioma were younger and received higher prescription doses than those without (mean ages of 43.5 and 47.1 years, and mean EQD2 doses of 55.7Gy and 53.9Gy, respectively), a categorical variable, *Glioma*, was included in the model. The interactions between dose and the clinical factors of age, sex and existence of edema were also tested. To identify clusters of significant predictors, a heatmap consisting of a matrix of p values associated with predictors was created for each tested linear model. Post-hoc pairwise Student's t-tests were performed to detect significant temporal changes in

AD/RD at each follow-up comparing to baseline values based upon dose-response patterns of the fibers. A p-value of 0.05 or less was considered as statistically significant.

Results

Of 33 patients, the median dose was 54Gy (Table 1). Four patients received concurrent chemotherapy with temozolomide. Thirteen patients had edema seen on pre-RT MRI.

Our approach achieved a mean Jaccard Similarity Index (JSI) of 0.82±0.04 over all WM bundles from 33 patients, equivalent to 90% of volume overlap of the same bundle tracked longitudinally. Compared to a traditional manual tracking method, the mean JSI was 0.64±0.09 (equivalent to 56% overlap) from three randomly selected patients, indicating high repeatability and robustness of our method.

Dose-Response Patterns

Twelve WM bundles had a significant main dose effect on longitudinal AD/RD changes (Table 2), in which a decrease in AD or RD was associated with a high dose.

Among 12 bundles, two dose-response patterns were observed, and examples are illustrated in heatmaps of Figure 3. The first pattern was that AD/RD changes were significantly associated with the *95%ile* and *90%ile* doses (maximum dose) but not the *mean dose*, referred as a *max-dose* pattern, suggesting a serial-structure response. The *max-dose* pattern included nine long inter-cortical association bundles, such as the inferior fronto-occipital fasciculus (IFOF), the inferior longitudinal fasciculus (ILF) and the cingulum cingulate at the hippocampus (CCH), and the main thalamo-cortical projection bundle of the anterior thalamic radiata (ATR).

The second pattern included three short-range association bundles, bilateral uncinate fasciculus (UNC) and the right arcuate fasciculus (AF), in which AD/RD changes were significantly associated with the mean dose and to a less extent with the maximum dose (Table 2), referred as a *multi-dose* pattern (Figure 3B). No significant dose-DTI correlation were observed in 10 other bundles (referred as the *non-sig* group)

Further analyses revealed that percentage volumes of fiber bundles receiving high doses (>45Gy) were different between bundles sensitive to the *max-dose* and the *multi-dose*. For patients whose bundles received high doses, approximately 68% and 40% of the bundle volume were exposed to high-dose for bundles sensitive to the *multi-dose* (e.g., the UNC) and to the *max-dose* (e.g., the IFOF), respectively. Given that large portions of the three short-range bundles were exposed to high doses, the effect of the maximum dose was not quite differentiable from the mean dose, and the observation of sensitivity to multi-dose levels might be due to the volume average effect of an actual serial structure.

Longitudinal DTI Changes

To evaluate dose-dependent temporal AD and RD changes, fiber bundles were first sorted by dose-response patterns (*max-dose*, *multi-dose*, and *non-sig*). Patient data of each bundle were then sorted into three dose-subgroups of low (<20Gy), medium (20-45Gy) and high

(>45Gy), according to the *95%ile dose* value if belonged to the *max-dose* or *non-sig* group, or according to the *mean dose* if belonged to the *multi-dose* group.

For the *max-dose* group, average AD and RD (Figures 4A and C) decreased significantly and progressively from pre-RT to 18 months post-RT at both medium and high doses. The decrease in average AD at high dose reached 3.9% (p=0.03) 18 months post-RT. Five bundles had an average decrease in AD more than 6% at 18 months post-RT, of which the right posterior IFOF had an average decrease of 11.5%. For the *multi-dose* group, average AD and RD decreased progressively, and reached significance at the high-dose level 18 months post-RT, in which the average reduction in AD was 7.0% with a maximum decrease of 10.7% seen in the right UNC (p=0.03). For the *non-sig* group, there were no significant AD/RD changes over time at any dose level.

As an example of individual bundles, the IFOF (from the *max-dose* group), the UNC (from the *multi-dose* group) and the genu of corpus callosum (GCC) (from the *non-sig* group) had a significant decrease in AD by 5.3%, 9.0% and 4.5% at the high-dose level 18 months post RT ($p<0.05$) respectively (Figure 4B).

Effects of Clinical Factors

Co-variables of glioma and interactions of dose with edema, age and sex significantly affected AD/RD changes within 6, 9, 4 and 5 WM bundles ($P<0.05$), respectively. After controlling dose and pathology (glioma vs non-glioma), age showed an interaction effect with dose, as AD/RD changed greater in elderly than in younger patients when received the same dose. Female patients had larger reductions in AD/RD than males given the same dose, consistent with previous observations (25-27) where sex-dependent differences in hippocampal plasticity as well as sex hormone (26) were reported as contributing factors to higher mortality and morbidity in females due to radiation-induced injury (27). Patients with glioma had a larger reduction in AD/RD than those without, possibly due to compromise of normal appearing WM by infiltrating glioma cells. Edema modulated dose effect and caused less decreases in AD/RD in patients with edema than those without. However, the edema effect was only apparent up to 1 month post-RT, and was diminished 6 months post-RT.

Discussion

In this study, an atlas-based, automated WM tractography analysis was implemented to investigate temporal and dose-response patterns of 22 major WM bundles. This approach allowed us to quantify DTI changes along individual bundles over time and relate them to received doses. We found that long inter-cortical association WM bundles responded to the maximum dose, like a typical serial structure, which has not been reported before. Also, we observed a dose-dependent progressive decrease in AD over time post-RT. Furthermore, aging and female sex increased sensitivity of WM to radiation dose. This study is the first necessary step toward developing a predictive model of a cognitive task by responses to radiation dose of individual WM bundles involved in neural network, and to help provide guidance for dose sparing of critical functional networks to preserve cognitive function in the future.

White matter response to radiation has been studied previously. The ROI-based approach, although used frequently, limits the ability to understand the dose-response of WM bundles beyond the mean dose in ROIs. It is also an error-prone and inefficient task to use a conventional ROI-based analysis to quantify temporal and spatial changes in the whole brain WM from 33 patients who had six longitudinal DTI scans. Therefore, we implemented an atlas-based tractography method to segment the whole volumes of 22 major WM bundles in the brain. This approach allowed us to test whether WM bundles respond to the maximum or mean dose. Our data indicate that nine long association or projection WM bundles responded to the maximum dose, suggesting a radiobiologic serial structure. The three short-range associated bundles, a large portion of which (up to an average of 68% of volumes) received high doses, were sensitive to both the mean and maximum doses, possibly due to the average volume effect of doses over a serial structure. Therefore, it could be equally important to avoid the high maximum dose and mean dose when short fibers have more than 50% of fiber length received high doses. WM bundles either receive high doses spreading from the PTV or pass through the PTV. Possibility for dose sparing of WM bundles should be future studies. Nevertheless, our findings provide a new insight on how to model brain normal tissue toxicity and redistribute doses to spare functional networks.

This study, as well as previous studies (10, 14), demonstrated a progressive decrease in AD over time. We hypothesize that this is due to astrogliosis. Progressive reactive astrogliosis (28-30) is a predominant histology after the early delayed phase (one month post-RT) with a marked increase of microglial cells and astrocytes as well as extensive cellular hypertrophy (17, 30). Increased extracellular matrix and astrocytic proliferation increase tortuosity and therefore reduce extracellular axial diffusion. Cellular hypertrophy distorts intracellular microtubule and consequently restricts intracellular axial diffusion. In contrast, both increase and decrease trends of RD post-RT were reported previously. Axon demyelination can cause RD increase (15, 18), while re-myelination can reverse the direction change in RD. Wang and colleagues (17) reported an initial RD decrease in rats up to 24 weeks post-RT due to astrogliosis. Given multiple competitive mechanisms (astrogliosis, demyelination and re-myelination), radiation-induced RD changes are most likely time-sensitive and subject-specific.

This study is not without limitations. One of limitations is DTI was acquired from different scanners with comparable protocols, which would increase inter-subject variations of DTI measurements (31, 32) and decrease statistical power. To minimize system-dependent bias, we acquired all DTI of the same patient from the same scanner, and also used percentage changes for analysis. Additional regression analysis with scanner as an independent variable did not reveal any significant scanner effect. Multiple comparison corrections were not applied due to the exploratory nature of this preliminary study. It is reassuring that all significant dose-ΔDTI% correlations before correction follow the consistent trend in contrast to random signs of correlations that are typically associated with true Type I errors. Also, edema decreases FA to <0.2. We limited fiber tracking to voxels with FA>0.2 to avoid edema and also used the JHU Atlas to further remove aberrant fibers. Nevertheless, edema usually subsided one-month post-RT. Corticosteroids also affects DTI changes. However, the findings after 6 months post-RT are less affected by edema and corticosteroids, as no patients received corticosteroids during that period. The ten fiber bundles that are found to

have no significant dose effect could likely be due to the dose spatial distribution in this sample, instead of dose sensitivity. Nevertheless, the dose-response pattern of WM bundles observed is hypothesis-generating for future study.

The major finding of this study, that the elongated association and projection fiber bundles respond like a serial structure, could provide a new insight on dose planning for long-term survivors to preserve critical cognitive functions. In current clinical practice, limited guidelines (33) are available to avoid necrosis and to spare brainstem and optic nerves/chiasm. Sparing critical WM fibers to reserve cognitive function, which is achievable by IMRT/VMAT techniques, has not traditionally been considered. The 12 fiber bundles that show significant dose effects (Table 2) are known to be essential parts of neural networks for executive functions, working memory and decision making (34, 35). Observed changes in these fibers are consistent with declines in executive and attentional functions observed in previous large-scale clinical trials of low-grade gliomas (5, 6). Whether dose-dependent longitudinal DTI changes in WM bundles are predictive and have a complimentary value to clinical factors (e.g., dosimetric parameters, age, sex, and pathology) for neurocognitive dysfunction merits future study.

Acknowledgments

This study was supported in part by NIH RO1 NS064973.

References

1. Sheline G. Radiation therapy of brain tumors. Cancer. 1977; 39:873–881. [PubMed: 837351]
2. Tofilon PJ, Fike JR. The radioresponse of the central nervous system: A dynamic process. Radiat Res. 2000; 153:357–380. [PubMed: 10798963]
3. Soussain C, Ricard D, Fike JR, et al. CNS complications of radiotherapy and chemotherapy. Lancet. 2009; 374:1639–151. [PubMed: 19897130]
4. Greens-Schloesser D, Robbins ME, Peiffer AM, et al. Radiation-induced brain injury: a review. Front Oncol. 2012; 2:73.doi: 10.3389/fonc.2012.00073 [PubMed: 22833841]
5. Klein M, Heimans JJ, Aaronson NK, et al. Effect of radiotherapy and other treatment-related factors in midterm to long-term cognitive sequelae in low-grade gliomas: a comparative study. Lancet. 2002; 360:1361–1368. [PubMed: 12423981]
6. Douw L, Klein M, Fagel SSA, et al. Cognitive and radiological effects of radiotherapy in patients with low-grade glioma: long-term follow-up. Lancet Neurol. 2009; 8:810–818. [PubMed: 19665931]
7. Kitahara S, Nakasu S, Murata K, et al. Evaluation of treatment-induced cerebral white matter injury by using diffusion-tensor MR imaging: initial experience. AJNR Am J Neuroradiol. 2005; 26:2200–2206. [PubMed: 16219822]
8. Chapman CH, Nazem-Zadeh M, Lee OE, et al. Regional variation in brain white matter diffusion index changes following chemoradiotherapy: a prospective study using tract-based spatial statistics. PLoS One. 2013; 8:e57768. [PubMed: 23469234]
9. Nagesh V, Tsien CI, Chenevert TL, et al. Radiation-induced changes in normal-appearing white matter in patients with cerebral tumors: A diffusion tensor imaging study. Int J Radiat Oncol Biol Phys. 2008; 70:1002–1010. [PubMed: 18313524]
10. Haris M, Kumar S, Raj MK, et al. Serial diffusion tensor imaging to characterize radiation-induced changes in normal-appearing white matter following radiotherapy in patients with adult low-grade gliomas. Radiat Med. 2008; 26:140–150. [PubMed: 18683569]

11. Chapman CH, Nagesh V, Sundgren PC, et al. Diffusion tensor imaging of normal-appearing white matter as biomarker for radiation-induced late delayed cognitive decline. Int J Radiat Oncol Biol Phys. 2012; 82:2033–2040. [PubMed: 21570218]
12. Hope TR, Vardal J, Bjornerud A, et al. Serial diffusion tensor imaging for early detection of radiation-induced injuries to normal-appearing white matter in high-grade glioma patients. J Magn Reson Imaging. 2015; 41:414–423. [PubMed: 24399480]
13. Khong PL, Kwong DL, Chan GC, et al. Diffusion-tensor imaging for the detection and quantification of treatment-induced white matter injury in children with medulloblastoma: A pilot study. AJNR Am J Neuroradiol. 2003; 24:734–740. [PubMed: 12695214]
14. Hua C, Merchant TE, Gajjar A, et al. Brain tumor therapy-induced changes in normal-appearing brainstem measured with longitudinal diffusion tensor imaging. Int J Radiat Oncol Biol Phys. 2012; 82:2047–2054. [PubMed: 21664060]
15. Song SK, Sun SW, Ramsbottom MJ, et al. Demyelination revealed through MRI as increased radial (but unchanged axial) diffusion of water. Neuroimage. 2002; 17:1429–1436. [PubMed: 12414282]
16. Sun SW, Liang HF, Le TQ, et al. Differential sensitivity of in vivo and ex vivo diffusion tensor imaging to evolving optic nerve injury in mice with retinal ischemia. Neuroimage. 2006; 32:1195–1204. [PubMed: 16797189]
17. Wang S, Wu EX, Qiu D, et al. Longitudinal diffusion tensor magnetic resonance imaging study of radiation – induced white matter damage in a rat model. Cancer Res. 2009; 69:1190–1198. [PubMed: 19155304]
18. MacDonald CL, Dikranian K, Bayly P, et al. Detects Experimental Traumatic Axonal Injury and Indicates Approximate Time of Injury. J Neurosci. 2007; 27:11869–11876. [PubMed: 17978027]
19. Mori S, Crain BJ, Chacko VP, et al. Three-dimensional tracking of axonal projections in the brain by magnetic resonance imaging. Ann Neurol. 1999; 45:265–269. [PubMed: 9989633]
20. Hua K, Zhang J, Wakana S, et al. Tract probability maps in stereotaxic spaces: analysis of white matter anatomy and tract-specific quantification. NeuroImage. 2008; 39(1):336–347. [PubMed: 17931890]
21. Alexander DC, Pierpaoli C, Basser PJ, et al. Spatial transformation of diffusion tensor magnetic resonance images. IEEE Trans Med Imaging. 2001; 20:1131–1139. [PubMed: 11700739]
22. Wakana S, Caprihan A, Panzenboeck MM, et al. Reproducibility of quantitative tractography methods applied to cerebral white matter. Neuroimage. 2007; 36:630–644. [PubMed: 17481925]
23. Basser PJ, Pajevic S, Pierpaoli C, et al. In vivo fiber tractography using DT-MRI data. Magn Reson Med. 2000; 44:625–632. [PubMed: 11025519]
24. Yeatman JD, Weiner KS, Pestilli F, et al. The Vertical Occipital Fasciculus: A Century of Controversy Resolved By In Vivo Measurements. Proc Natl Acad Sci. 2014; 111:E5214–5223. [PubMed: 25404310]
25. Farjam R, Pramanik P, Madhava A, et al. A radiation-induced hippocampal vascular injury surrogate marker predicts late neurocognitive dysfunction. Int J Radiat Oncol Biol Phys. 2015 accepted for publication.
26. Raber J. Unintended effects of cranial irradiation on cognitive function. Toxicol Pathol. 2010; 38:198–202. [PubMed: 19880825]
27. National Research Council (US). Committee to assess health risks from exposure to low level of ionizing radiation Heath risks from exposure to low levels of ionizing radiation: BEIR VII Phase 2. Washington, DC: Nationation Academic Press; 2006.
28. Greene-Schloesser D, Moore E, Robbins ME. Molecular pathways: radiation-induced cognitive impairment. Clin Cancer Res. 2013; 19:2294–2300. [PubMed: 23388505]
29. Reinhold HS, Calvo W, Hopewell JW, et al. Development of blood vessel-related radiation damage in the fimbria of the central nervous system. Int J Radiat Oncol Bio Phys. 1990; 18:37–42. [PubMed: 2298633]
30. Yang I, W SL, Liang JC, et al. Time-dependent atroglial changes after γ knife radiosurgery in the rat forebrain. Neurosurgery. 2000; 47:407–415. [PubMed: 10942014]
31. Zhu T, Hu R, Qiu X, et al. Quantification of accuracy and precision of multi-center DTI measurements: a diffusion phantom and human brain study. Neuroimage. 2011; 56:1398–1411. [PubMed: 21316471]

32. Nazem-Zadeh M, Chapman CH, Lawrence TS, et al. Uncertainty in assessment of radiation-induced diffusion index changes in individual patients. Phys Med Biol. 2013; 58:4277–4296. [PubMed: 23732399]

33. Marks LB, Yorke ED, Jackson A, et al. Use of normal tissue complication probability models in the clinic. Int J Radiat Oncol Biol Phys. 2010; 76:S10–S19. [PubMed: 20171502]

34. Schmahmann JD, Pandya DN. The complex history of the fronto-occipital fasciculus. J Hist Neurosci. 2007; 16:362–377. [PubMed: 17966054]

35. Jones DK, Christiansen KF, Chapman RJ, et al. Distinct subdivisions of the cingulum bundle revealed by diffusion MRI fiber tracking: Implications for neuropsychological investigations. Neuropsychologia. 2013; 51:67–78. [PubMed: 23178227]

Summary

Neurocognitive function is supported by white matter (WM) fiber bundles in the neural network. WM bundles are highly susceptible to radiation damage. In this study, we found that elongated WM fiber bundles responded to the received maximum dose rather than the mean dose, much like a typical serial-structure. These findings provide a new framework on how to spare dose for critical functional networks to preserve cognitive function.

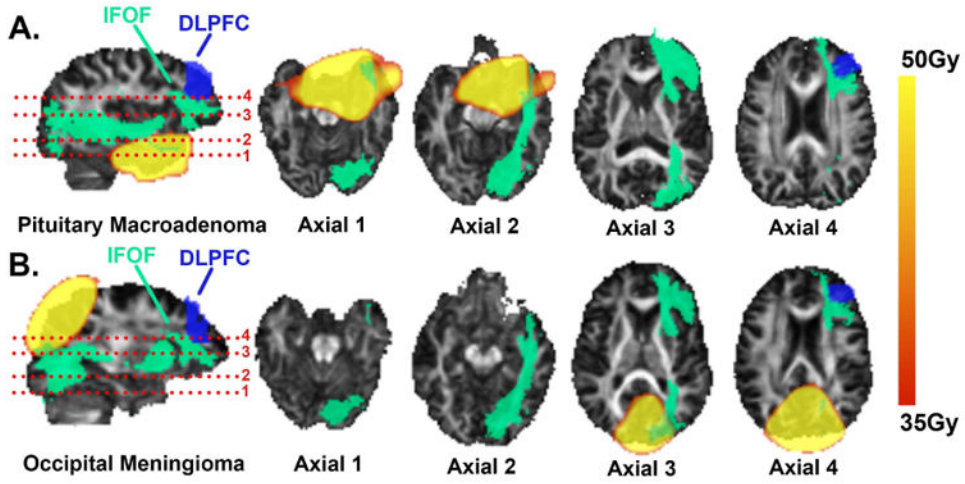

Figure 1.

Examples (with scalp and skull removed) of different high-dose regions of two patients who had neurocognitive declines related to the dorsolateral prefrontal cortex (DLPFC). High-dose regions were distal to the DLPFC but overlapped at different sections of the inferior fronto-occipital fasciculus (IFOF), an essential part of the DLPFC neural network.

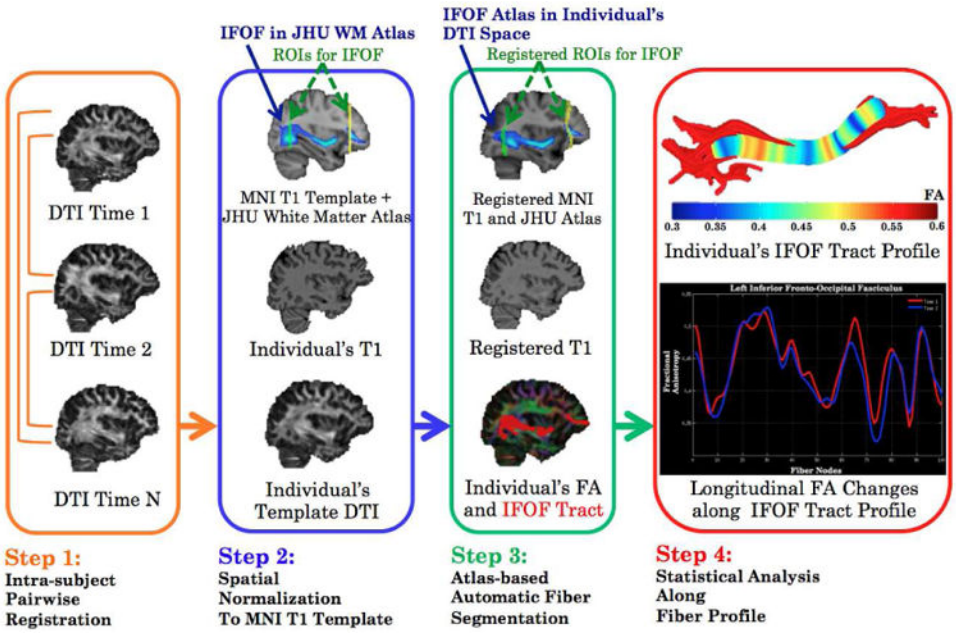

Figure 2.
Flow chart of the atlas-based, automated tractography method.

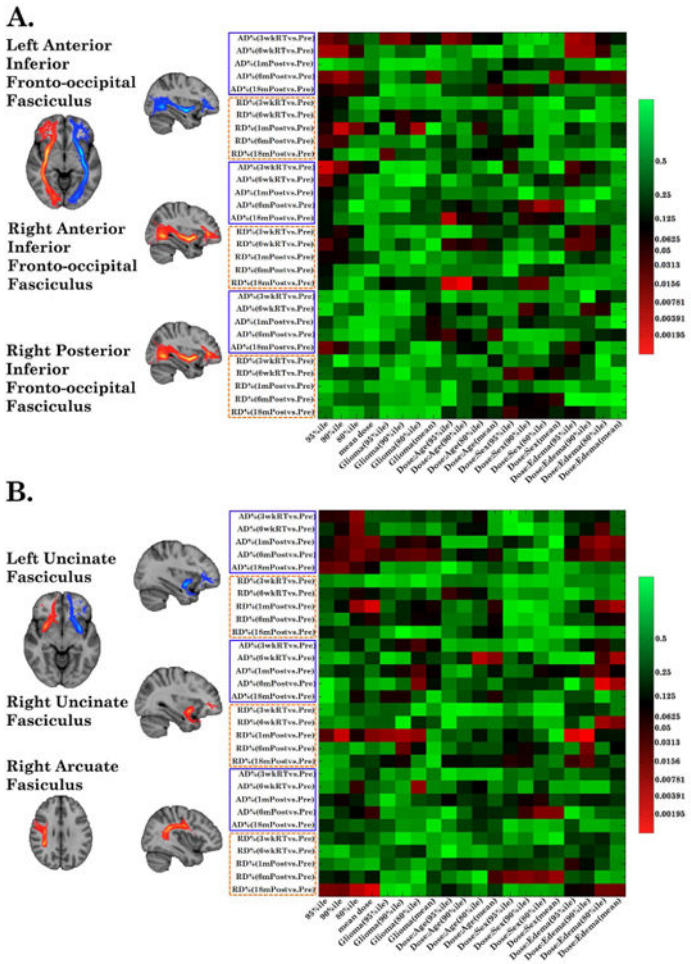

Figure 3.

Heatmaps of linear fixed-effect models. The vertical axis represents dependent variables (sorted first by ΔAD%/ΔRD% then by time points). The horizontal axis depicts independent variables of four dose metrics, glioma, and three interaction co-variables. Examples of WM bundles responded to the maximum dose and to both the maximum and mean doses are displayed in (A) and (B), respectively.

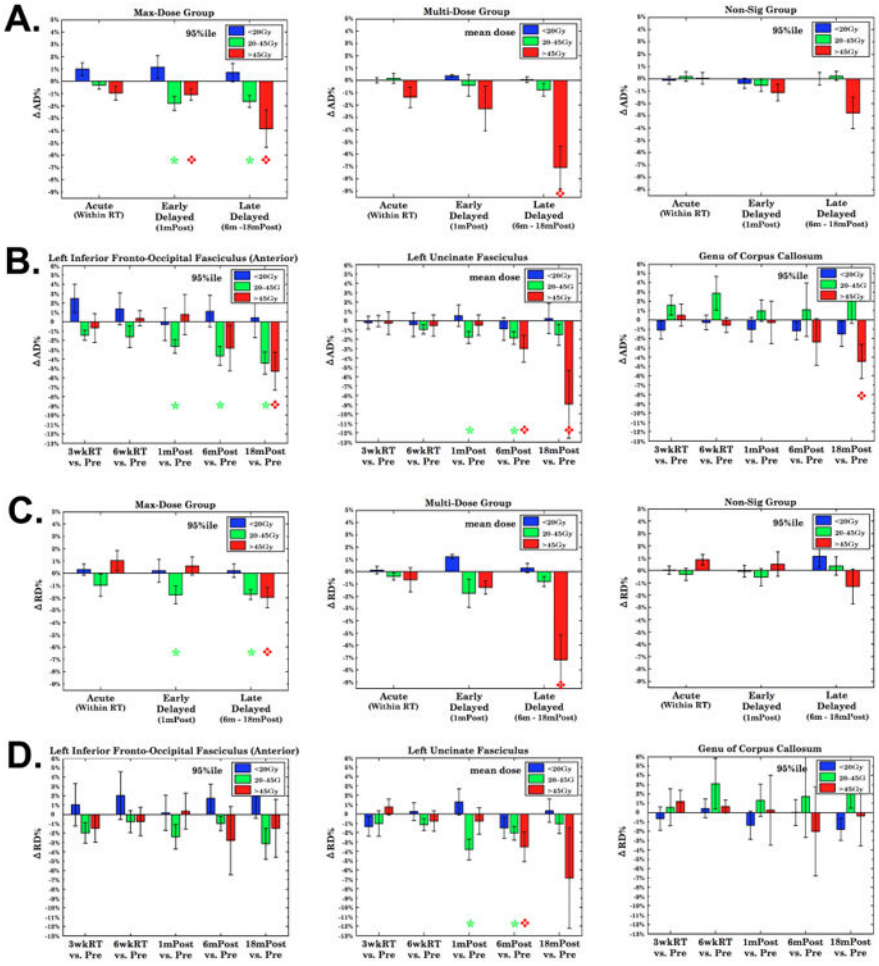

Figure 4.

Dose-dependent longitudinal ΔAD% and ΔRD% for the *Max-Dose* (left), *Multi-Dose* (middle) and *Non-Sig* group (right column). ΔAD%/ΔRD% were averaged over voxels receiving doses higher than the 95%ile on bundles for the *Max-Dose* and *Non-Sig* groups, and over all voxels for the *Multi-Dose* group. ΔAD%/ΔRD% in 4A and 4C were further averaged over the bundles within each group. ΔAD% (4B) and ΔRD% (4D) from the IFOF, UNC and GCC represent the three abovementioned groups. Red diamonds and green stars: significant at the time point for respective high- and medium-dose levels.

Table 1

Patient characteristics

Patient ID	Age(y)	Gender	Tumor Type	Anatomic Tumor location	Prescribed Dose (Gy)	Edema	Scans
1	34	M	Grade II gemistocytic astrocytoma	Right temporal lobe	57.6	Yes	6/6
2	55	M	Meningioma	Left temporal lobe	54	Yes	6/6
3	72	M	Pituitary macroadenoma	Suprasellar	50.4	No	5/6
4	39	M	Grade II mixed oligoastrocytoma	Right inferior frontal lobe	57.6	Yes	6/6
5	29	M	Craniopharyngioma	Suprasellar	55.8	No	5/6
6	44	M	Pituitary macroadenoma	Suprasellar	50.4	No	6/6
7	25	F	Grade II low grade glioma	Left temporal lobe	54	Yes	6/6
8	64	M	Pituitary macroadenoma	Suprasellar	50.4	No	6/6
9	56	M	Grade II astrocytoma	Left frontal lobe	54	Yes	5/6
10	59	F	Null-cell pituitary adenoma	Suprasellar and right temporal lobe	50.4	No	5/6
11	53	F	Meningioma	Suprasellar and left temporal	55.8	No	6/6
12	27	F	Grade II oligoastrocytoma	Left frontal temporal lobe	54	Yes	6/6
13	56	M	Null-cell pituitary adenoma	Suprasellar	50.4	No	6/6
14	44	F	Null-cell pituitary adenoma	Suprasellar	50.4	No	6/6
15	44	M	Grade II diffuse oligodendroglioma	Right parietal occipital lobe	54	Yes	6/6
16	47	F	Pituitary macroadenoma	Suprasellar	50.4	No	6/6
17	54	F	Meningioma	Middle parietal and occipital lobe	54	No	5/6
18	56	F	Grade II gemistocytic astrocytoma	Right superior frontal lobe	54	Yes	6/6
19	48	M	Pituitary macroadenoma	Suprasellar	50.4	No	6/6
20	38	F	Meningioma	Cerebellum and Occipital lobe	54	No	6/6
21	48	M	Meningioma	Right inferior temporal lobe	54	No	6/6
22	50	M	Grade II diffuse astrocytoma	Left temporal lobe	57.6	Yes	6/6
23	47	M	Null-cell pituitary adenoma	Suprasellar	54	No	6/6
24	31	F	Craniopharyngioma	Suprasellar	55.8	No	6/6
25	39	F	Adenocystic carcinoma	Suprasellar	70	No	5/6
26	58	M	Grade I hemangioblastoma	Right inferior temporal lobe	57.6	No	4/6
27	53	F	Meningioma	Superior parietal lobe	54	No	6/6
28	43	F	Grade II diffuse astrocytoma	Left temporal and frontal lobe	54	Yes	4/6

Patient ID	Age(y)	Gender	Tumor Type	Anatomic Tumor location	Prescribed Dose (Gy)	Edema	Scans
29	57	M	Pituitary macroadenoma	Suprasellar	50.4	No	6/6
30	41	F	Meningioma	Right temporal lobe	54	Yes	6/6
31	62	M	Meningioma	Left temporal and frontal lobe	54	Yes	6/6
32	62	F	Anaplastic astrocytoma	Left frontal lobe	60	Yes	5/6
33	33	M	Germinoma	Right superior frontal lobe	45	No	5/6

Table 2

Coefficients of the main dose effect on DTI changes from the multivariate linear fixed-effect model

WM Tracts	95%ile (mean) dose vs. ΔAD%					95%ile (mean) dose vs. ΔRD%				
	3wkRT	6wkRT	1mPost	6mPost	18mPost	3wkRT	6wkRT	1mPost	6mPost	18mPost
ATR_L	-0.16 (-0.12)	0.068 (0.081)	**-0.24** * (-0.11)	-0.028 (-0.065)	-0.11 (-0.17)	-0.0041 (0.022)	0.15 (0.094)	-0.058 (-0.046)	0.077 (0.049)	0.13 (-0.027)
ATR_R	**-0.15** * (-0.092)	-0.050 (-0.026)	-0.056 (-0.083)	-0.15 (-0.012)	-0.17 (-0.14)	-0.092 (-0.070)	-0.025 (-0.024)	-0.046 (-0.038)	-0.15 (-0.032)	-0.11 (-0.11)
CCH_L	-0.062 (-0.11)	-0.19 (0.029)	**-0.30** * (-0.19)	**-0.26** * (-0.23)	**-0.31** * (-0.17)	0.0082 (-0.070)	0.0033 (0.074)	-0.28 (-0.18)	-0.17 (-0.12)	-0.21 (-0.060)
CCH_R	-0.20 (-0.020)	-0.11 (-0.010)	-0.16 (-0.23)	**-0.33** ** (-0.088)	**-0.40** * (-0.36)	0.074 (0.16)	-0.054 (0.062)	0.042 (-0.10)	-0.21 (-0.14)	-0.36 (-0.069)
IFOF_A_L	**-0.15** * (-0.055)	**-0.22** ** (-0.045)	0.0088 (0.062)	**-0.28** * (-0.089)	-0.25 (-017)	-0.15 (-0.014)	-0.17 (-0.040)	-0.22 (-0.21)	**-0.37** * (-0.099)	-0.30 (-0.055)
IFOF_A_R	**-0.24** ** (-0.11)	**-0.17** * (-0.014)	-0.18 (-0.017)	-0.16 (-0.023)	-0.16 (-0.042)	-0.10 (-0.017)	**-0.19** * (-0.019)	-0.21 (-0.11)	-0.21 (-0.012)	-0.18 (-0.12)
IFOF_P_R	-0.031 (0.023)	-0.011 (0.011)	-0.085 (0.011)	-0.060 (-0.0036)	**-0.32** * (-0.087)	-0.088 (0.025)	0.077 (0.13)	0.014 (-0.033)	0.051 (0.17)	-0.12 (0.18)
ILF_L	-0.044 (-0.080)	0.011 (-0.023)	-0.039 (-0.076)	**-0.23** * (**-0.21** *)	-0.10 (-0.16)	0.11 (0.054)	0.034 (0.063)	0.030 (0.022)	-0.12 (-0.12)	-0.036 (-0.073)
ILF_R	-0.035 (0.014)	-0.044 (-0.0094)	-0.092 (-0.014)	-0.033 (0.031)	0.0036 (-0.15)	-0.091 (0.030)	-0.11 (0.0027)	**-0.22** ** (-0.11)	0.012 (0.20)	-0.24 (-0.26)
AF_R	0.028 (0.15)	0.056 (0.13)	0.17 (0.095)	0.078 (**-0.24** *)	-0.23 (-0.19)	-0.13 (-0.15)	0.049 (0.081)	-0.086 (0.036)	0.18 (0.21)	**-0.37** ** (**-0.53** **)
UNC_L	**-0.12** * (-0.052)	-0.073 (-0.067)	-0.11 (**-0.15** **)	**-0.18** * (**-0.16** *)	**-0.30** * (-0.22)	-0.059 (0.0054)	-0.064 (-0.087)	-0.10 (**-0.26** **)	-0.094 (**-0.16** *)	-0.18 (-0.18)
UNC_R	-0.058 (-0.034)	0.040 (-0.065)	-0.078 (-0.054)	0.0031 (-0.034)	-0.0042 (-0.10)	-0.019 (-0.052)	-0.060 (-0.080)	**-0.14** * (**-0.16** **)	0.074 (-0.075)	0.047 (-0.16)

(1). Abbreviation for fibers (same abbreviations used from all tables and figures)**:** A – Anterior, P – Posterior, L – Left, R – Right. AF -Arcuate Fasciculus, ATR – Anterior Thalamic Radiata, CCH - Cingulum Cingulate at Hippocampus, IFOF – Inferior Fronto-Occipital Fasciculus, ILF – Inferior Longitudinal Fasciculus, UNC – Uncinate Fasciculus.

(2). Bold fonts indicate significant correlations:

* $p<0.05$,

** $p<0.01$